Indian Journal of Pure & Applied Physics
Vol. 56, January 2018, pp. 19-25

Investigation of ZnO nanoparticles for their applications in wastewater treatment and antimicrobial activity

Neha Rana[a,b], Kalyan S Ghosh[c], Subhash Chand[a] & Arvind K Gathania[a]*

[a]Department of Physics, National Institute of Technology Hamirpur, Hamirpur 177 005, India

[b]Department of Physics, Shri Guru Granth Sahib World University, Fatehgarh Sahib 140 407, India

[c]Department of Chemistry, National Institute of Technology Hamirpur, Hamirpur 177 005, India

Received 20 February 2017; accepted 2 November 2017

The photocatalytic as well as the antimicrobial activity of the synthesized ZnO nanoparticles (ZnO-NPs) through solution based approach have been presented in this study. ZnO-NPs have been characterised by thermogravimetry/differential thermal analysis (TG/DTA), ultraviolet-visible (UV–Vis), Fourier transform infrared (FTIR) and Raman spectroscopy. Raman studies confirm that it has stable wurtzite structure. FTIR spectrum confirms the Zn–O band at ~460 cm^{-1}. Optical studies reveal that the optical band gap value increases with increasing annealing temperature. The photocatalytic activity of the ZnO-NPs has been evaluated for removal of pollutants from wastewater by measuring COD and BOD. Results show that ZnO-NPs are capable of working efficiently for waste water treatment. ZnO-NPs also demonstrate antimicrobial activity against gram-positive and gram-negative bacterial strains.

Keywords: ZnO-NPs, Thermogravimetry/differential thermal analysis, Optical band gap, Photocatalytic, Wastewater treatment, Antimicrobial

1 Introduction

Zinc oxide nanostructures have attracted much interest in recent years because of their diversified technological applications in solar cells, catalysts, waveguides, transparent thin-film transistors, piezoelectric transducers and actuators, surface wave acoustic devices, gas sensors and photonic crystals with tunable band gaps[1-7]. Beside above mentioned applications, semi-conductive particles, such as TiO_2, Nb_2O_5 and ZnO[8-12] have also been explored for efficient removal of organic pollutants in water and hold good bio-compatibility to human cells. Polluted water from industries and colonies as well as bacterial infection related diseases are very alarming health problems allure the intellectual's attention around the globe. Researchers propose various mechanisms to deal with such threats. Dhiman *et al*.[10] have studied the core-shell composite microspheres of TiO_2-SiO_2 for photocatalytic removal of organic pollutant[9]. ZnO is a superior alternative to a standard TiO_2 photocatalyst due to comparable band gap, i.e., 3.2 eV. It has higher quantum yield for peroxide production and larger photocatalytic efficiencies[11-13]. The large fraction of the solar spectrum absorption in ZnO as compared to other photocatalysts also accounts for its better photocatalytic activity[14].

Nanostructures of ZnO also exhibit superior photocatalytic applications as compared to the bulk counterpart due to the larger surface area which results in the increase of surface reactivity. In addition, the higher photocatalytic reactions rate in nano-regime in comparison to their bulk counterparts also causes an increase in the efficiency of photocatalyst[10,15]. Recently a number of methods have been developed to synthesize ZnO nanostructures such as thermal decomposition[16], microemulsion[17], sol–gel[18], gas phase reaction[19], spray pyrolysis[20], hydrothermal synthesis[21,22] and precipitation[23]. Among these synthesis methods, the chemical method is found to be more convenient, less expensive and easy to tailor the chemistry of the nanostructures[24,25].

The aim of the present study is to investigate the optical properties of ZnO-NPs. Removal of pollutants from the in-house wastewater is achieved. Experiments are carried out in lab scale and efficiency is tested on the in-house wastewater collected from NIT Hamirpur campus. Antimicrobial activity is also demonstrated by the ZnO-NPs.

*Corresponding author (E-mail: akgathania@yahoo.com)

2 Experimental Details

Zinc acetate dihydrate ($Zn(CH_3COO)_2 \cdot 2H_2O$) is purchased from Merck (Purity ≥ 98%). Methanol is obtained from Sigma-Aldrich (Purity ≥ 99%) and lithium hydroxide (LiOH) is purchased from Otto (Purity 99%). All the chemicals are used without further purification. Two bacterial strains, staphylococcus aureus (S. aureus) and escherichia coli (E. coli) are from MTCC, Institute of Microbial Technology, Chandigarh and New England Bio labs, respectively. Other requirements for bacterial cultures, such as agar, yeast extract, beef extract, sodium chloride, tryptone, peptone and Petri-dishes get from Himedia.

$Zn(CH_3COO)_2 \cdot 2H_2O$ (0.25 M) solution was prepared in 200 mL methanol and refluxed at about 70 °C for 30 min under vigorous magnetic stirring to get a homogeneous solution. 0.25 M LiOH solution was added dropwise in 200 mL methanol for hydrolysis. This reaction mixture was then aged at 70 °C under continuous stirring under refluxing conditions for 2 h. Finally, the precipitates were washed and afterwards dried in a vacuum oven for 24 h. Synthesised samples were annealed at different temperatures (200, 300 and 400 °C) for 1 h in the air and used for further characterization.

The thermal stability of the ZnO-NPs has been investigated by TG/DTA (EXSTAR6000 TG/DTA 6300) in the temperature range 50−700 °C at a heating rate of 10 °C/min. FTIR studies are conducted using PerkinElmer Spectrum 65 spectrometer on compressed pellets prepared by mixing powder samples with potassium bromide (KBr). Raman spectroscopy is performed with an In Via Raman spectrophotometer (Renishaw) with $Ar^{/+}$ ion laser beam having a wavelength of 514 nm. Optical properties are investigated using a UV–Vis spectrometer (PerkinElmer, LAMBDA 750).

COD and BOD studies demonstrate the photocatalytic removal of pollutants from sewage wastewater with ZnO-NPs. Fresh in-house wastewater is collected from NIT Hamirpur campus. COD study uses a digestion method followed by colorimetric estimation. An appropriate amount of sample is taken from the digestion solution (Hach) and then the mixture is incubated for 120 min at 150 °C in a digestion unit (Hach, model DRB 200). COD concentrations are measured using a Hach DR 2700 spectrophotometer.

BOD study measures oxygen intake by microorganisms in a water sample at 20 °C during 5 days in dark using Hach HQ 30D BOD meter. BOD nutrient buffer is prepared using Hach reagent and used for dilution of water samples. The wastewater samples are put in BOD bottles and diluted with the nutrient buffer solution. Initial dissolved oxygen concentration is measured. After five days of incubation, the final dissolved oxygen concentration is also measured. The standard method of calculating BOD of the water samples is as:

$$\mathrm{BOD} = \frac{D_\mathrm{i} - D_\mathrm{f}}{P} \quad \ldots (1)$$

where, D_i is the initial dissolved oxygen content before incubation, D_f is the final dissolved oxygen content after incubation, P is the decimal volumetric fraction of the sample used.

The removal efficiency X (%) is calculated using the change of COD and BOD values of wastewater samples before and after treatment as:

$$X(\%) = \frac{(A_\mathrm{i} - A_\mathrm{t})}{A_\mathrm{i}} \times 100 \quad \ldots (2)$$

where A_i is the initial value of the parameter (COD /BOD) and A_t is the value of that parameter at different time intervals of wastewater treatment by ZnO-NPs.

For the antimicrobial activity of ZnO-NPs S. aureus (gram-positive) and E. coli (gram-negative) bacteria were selected. Gram-positive and gram-negative are cultured in suitable culture mediums at 37 °C. Bacterial cells are cultured initially in liquid media till the optical density ~ 0.8 at 600 nm. Five microliters of this cultured bacterial cells with and without ZnO-NPs (5 mg/ml) solution is dropped on an agar plate and incubated at 37 °C for 12 h. Bacterial cells without ZnO-NPs are used as a control. After 12 h of incubation, the antibacterial activity is evaluated by measuring the diameter (mm) of the grown bacteria colonies in the presence and absence of ZnO-NPs.

3 Results and Discussion

Figure 1 shows the TG/DTA curves of ZnO samples prepared and dried at room temperature**.** The TG curve can be divided into three distinct phases. The first weight loss of 2.7% in the temperature range

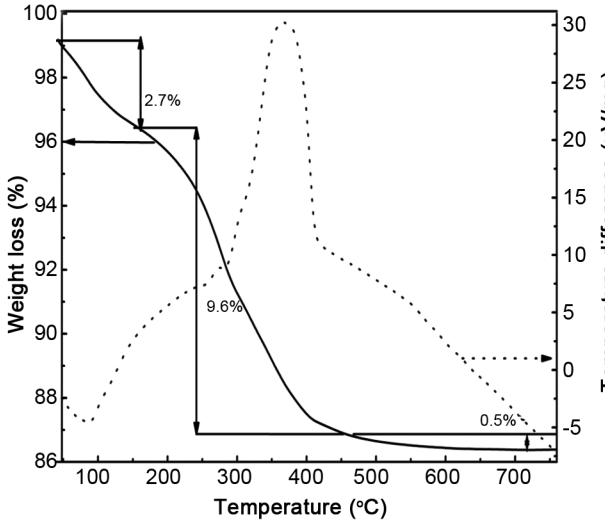

Fig. 1 — Thermogravimetric and differential thermal analysis of ZnO sample for temperatures up to 760 °C.

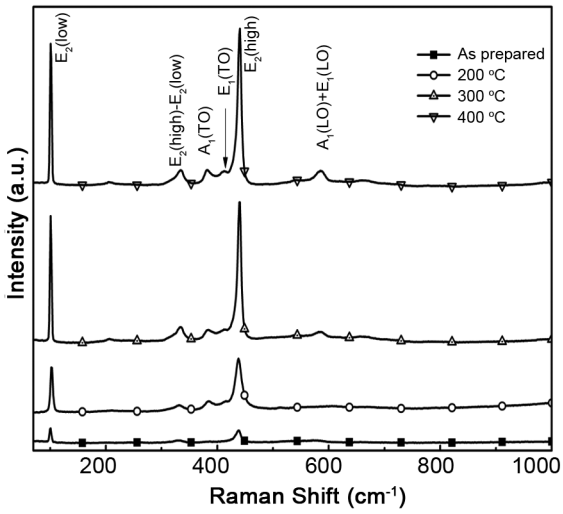

Fig. 2 — Raman spectra of the ZnO-NPs samples annealed at different temperatures.

from 40 to 150 °C is attributed to the release of the hygroscopic humidity, dehydration and dehydroxylation. The DTA curve shows an endothermic peak at 80 °C which also reflects the weight loss in the sample. Therefore, above 150 °C only ZnO and $Zn(CH_3COO)_2$ should exist in the system. The largest weight loss (9.6%) is in the second stage from 150 - 450 °C. It reflects a complete decomposition of the zinc acetate as shown below:

$$Zn(CH_3COO)_2 \rightarrow ZnO + (CH_3CO)_2 \quad \ldots (3)$$

Figure 1 reflects a strong exothermic peak at 367 °C due to crystallization of ZnO in the DTA curve. The mass of the sample reaches an approximately constant value above 450 °C. Another small weight loss of 0.5% is observed in the temperature interval 450–760 °C, which corresponds to the release of entrapped gases formed due to decomposition of acetate ions[26].

For wurtzite ZnO (space group *P*63*mc*) near the center of the Brillouin zone (k = 0) group theory predicts the existence of the following optical modes: $\Gamma_{opt} = A_1+E_1+ 2E_2+2B_1$. The $B1$ modes are silent, the E_2 modes are non-polar and Raman active, while A_1 and E_1 are polar modes and Raman as well as infrared active. Figure 2 shows the Raman spectra of the samples annealed at different temperatures. The observed peaks in these spectra are assigned to the Raman-active modes of the ZnO wurtzite crystal[27]. Two sharp dominating peaks corresponding to E_2 mode are observed in all the samples. It is also observed that the intensity of these peaks is increasing with an increase in annealing temperature for the samples. It indicates that the crystallization of the samples is becoming better with annealing.

Figure 3 shows the FTIR spectrum of as-prepared and further annealed ZnO-NPs. It illustrates a series of absorption bands in the range of 450–4000 cm^{-1}. The broad asymmetrical band positions at ~ 3300 cm^{-1} assigned to the O–H stretching mode for -COOH group in zinc acetate. Absorption bands at ~ 2880 and ~ 2940 cm^{-1} correspond to the C–H stretching vibrations of acetate. The bands appear between ~ 1400 and 1600 cm^{-1}, attributed to the stretching modes (symmetric and asymmetric) of the acetate group (-COOH). These groups adsorb on the surface of the nanoparticles during the synthesis process. The absorption band at ~ 1000 cm^{-1} is due to the C=O deformation mode of the acetate groups. It is pertinent to note that the intensity at these vibrational frequencies decreases at higher annealing temperatures, which suggests degradation of zinc acetate into its oxide at higher temperatures. The band positioned at ~460 cm^{-1} represents the bonding between Zn and O[28,29]. This also supports our earlier results that crystallization is improving with the increase in annealing temperature.

Figure 4 presents the absorption spectrum of ZnO-NPs at different annealing temperatures. The optical band gap of ZnO-NPs is estimating from using the Tauc's equation which demonstrates a relationship between absorption coefficient and the incident

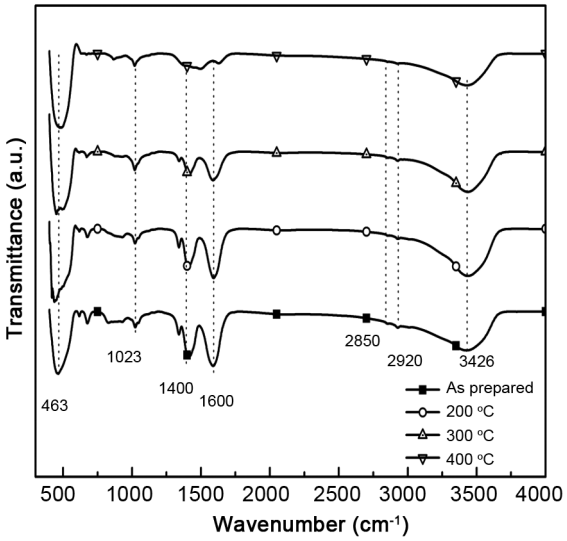

Fig. 3 — FTIR spectra of the as-prepared and annealed samples at different temperatures.

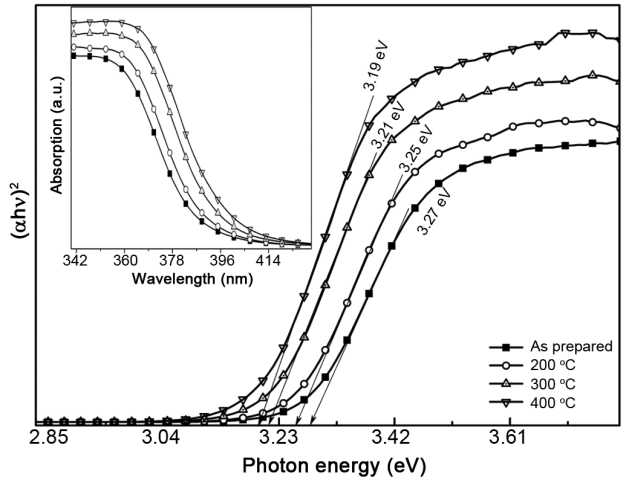

Fig. 4 — Absorption edge (inset) and $(\alpha h\nu)^2$ versus photon energy plots at different temperatures of ZnO-NPs samples.

photon energy of semiconductors and given as follows[30]:

$$(\alpha h\nu) = A(h\nu - E_g)^n \quad \ldots (4)$$

where α is the absorption coefficient, A is a constant, $h\nu$ is the photon energy, E_g is the optical band gap and n is ½ for direct band gap semiconductors..

An extrapolation of the linear region of a plot of $(\alpha h\nu)^2$ on the y-axis versus photon energy ($h\nu$) on the x-axis gives the value of the optical band gap (E_g), since $E_g = h\nu$ when $(\alpha h\nu)^2 = 0$. Figure 4 shows that the band gap of the prepared samples decreases from 3.26 to 3.13 eV as the absorption edge systematically shifts to the higher wavelength with increasing annealing temperature. The improvement in the crystallinity of the ZnO-NPs with increasing annealing temperature is responsible for a decrease in E_g[31].

The photocatalytic degradation of water contaminants carries out with our in-house wastewater. The photocatalysis is the generation of electron/hole pairs (e^- /h^+) by the promotion of an electron from the valence band (VB) to the conduction band (CB) on irradiation of ZnO-NPs with light ($h\nu \geq E_g$) as shown below:

$$\mathrm{ZnO} + h\nu \rightarrow \mathrm{ZnO}\,(e^-_{CB} + h^+_{VB}) \quad \ldots (5)$$

where h^+_{VB} is the hole generated in the VB and e^-_{CB} is the electron in the CB and $h\nu$ is the energy of light. After that, the charge carrier species can recombine and the absorbed energy dissipates as heat, or these species may migrate to the particle surface. The holes in the VB can act as the site for strong oxidation and can oxidize water (H_2O) molecules and hydroxyl (OH^-) groups. It results to generate the highly reactive pairs (ROS). ROS include peroxide (O_2^-), peroxide (H_2O_2) and hydroxyl ($OH^\bullet$) radical[32].

The detailed mechanism involves in this process is as follows. On irradiation sample with photons having energy greater than 3.3 eV, the electrons move from VB to CB. These electrons initiate photoreactions. Oxygen (O_2) molecules adsorbed on the surface is reduced by these electrons to form superoxide anion ($O_2^{\bullet-}$) radicals, which in turn react with H^+ to generate hydrogen peroxide ($HO_2^\bullet$) radicals. $HO_2^\bullet$ radicals will react with electrons and H^+ ions to produce molecules of H_2O_2. In addition, oxygen vacancies in the semiconductor crystals act as electron donors[33]. The additional electrons induced by these vacancies will promote the reactions to further yield $OH^\bullet$ radicals. These highly reactive $OH^\bullet$ radicals and H_2O_2 molecules have a strong oxidative potential for partial or complete decomposition of various organic, inorganic and microbial contaminants adsorbed on the photocatalyst surface[34]. Figure 5 illustrates the temporal evolution of COD and BOD removal efficiency of the wastewater by ZnO-NPs. It is worth noting that the removal efficiency increases with an increase in the irradiation/contact time, and then reaches a constant value reflects no further removal. The saturation after a certain time is due to the decrease of the available surface sites for adsorption of pollutant molecules. During the initial stage of

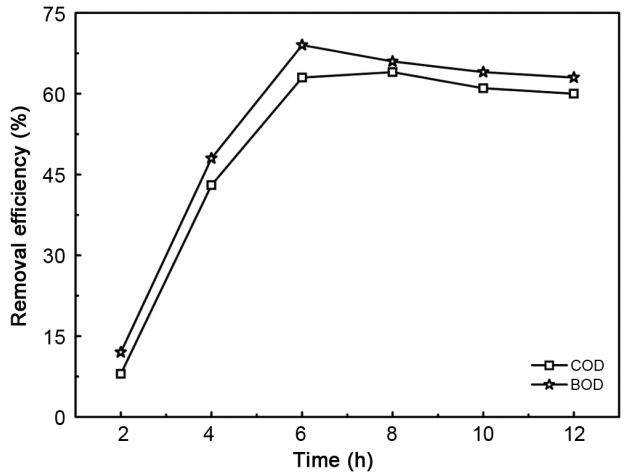

Fig. 5 — Photocatalytic removal of wastewater pollutant versus irradiation time.

adsorption there are many vacant surface sites available on the ZnO-NPs, but after some time the repulsive forces between the already adsorbed molecules do not support further adsorption[35].

Figure 6 shows the growth of the bacterial strains with and without ZnO-NPs. The results have been summarized in Table 1. It is seen that the growth is reduced to 26% in gram-negative bacterial strain whereas it is reduced significantly up to 45% in gram-positive bacterial strain after 12 h incubation. ZnO-NPs show better antimicrobial activity against the gram-positive bacterial strain. Figure 6(c) shows the structure of a bacterial cell. It contains membrane, nuclear materials, cell wall etc. The cell membrane lies inside the cell wall. It helps to maintain the osmotic pressure of the cytoplasm. Various possible

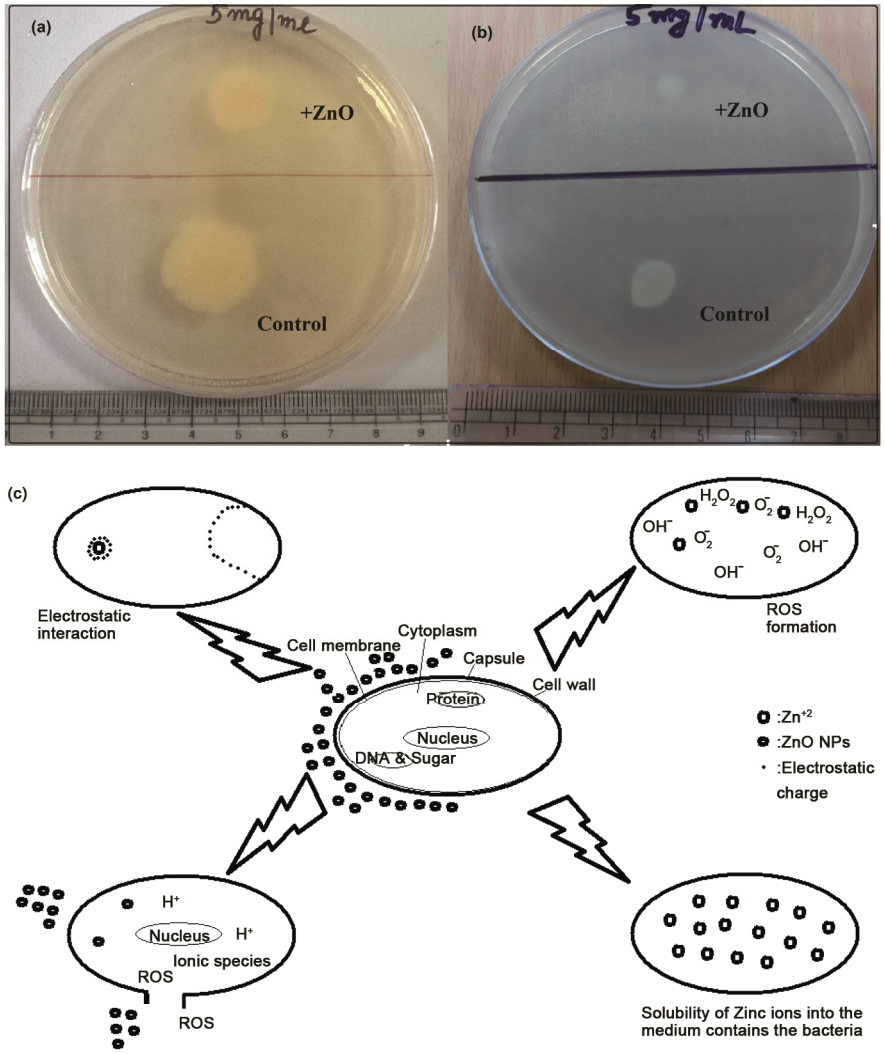

Fig. 6 — Strain growth with and without ZnO-NPs for (a) gram-negative and (b) gram-positive, and (c) various antimicrobial activity mechanisms of ZnO-NPs [38].

mechanisms involved in the antimicrobial activity of ZnO-NPs are depicted in Fig. 6(c). It results due to the production of ROS from ZnO-NPs. Such species leads to destruct the cellular components. There is internalization within the membrane. Superoxides and hydroxyl radical carry negative charges and due to this they can't penetrate into the membrane and always remain at the outer surface of the bacteria. However, H_2O_2 molecules pass through the cell wall. It injures and damages as well as destroys the cell. In the present case, ZnO-NPs are present in the growth media, it releases peroxides and covers the surface of bacteria. Greater the adsorption of H_2O_2 at the bacteria surface more is antimicrobial efficiency. Some earlier reports also support the better resistance of gram-negative bacteria[35,36]. The gram-negative bacteria have double cell membrane as compared to gram-positive bacterial strain. The outer membrane in gram-negative bacteria restricts the permeability of various molecules[37] which results in less growth reduction. Whereas single cell membrane in gram-positive bacterial strain can easily be damaged, this reflects its superiority for antimicrobial activity.

4 Conclusions

ZnO-NPs have been synthesized successfully by chemical route. Annealing of nanoparticles assists the removal of acetate impurities and moisture to get pure ZnO-NPs. The formation of ZnO-NPs is also confirmed by metal–oxygen vibration observed in the FTIR spectrum. The band gap of the ZnO-NPs is estimated using Tauc's equation. It is noticed that band gap exhibits a blue shift with the increase of annealing temperature of the samples. The present work also demonstrates that ZnO-NPs can be considered as a promising photocatalyst in the removal of the contaminant of wastewater. Antimicrobial studies show that ZnO-NPs exhibit better results with gram-positive bacterial strain as compared to gram-negative bacterial strain.

Acknowledgement

The authors thank NIT-Hamirpur for providing financial assistance and CMSE NIT Hamirpur for providing experimental facilities to carry out the present work.

References

1 Jagadish C & Pearton S, *Zinc oxide bulk, thin films and nanostructures,* (Elsevier), 2006.
2 Nickel N H & Terukov E, *Zinc oxide — A material for micro- and optoelectronic applications,* (Springer: Netherlands), 2005.
3 Özgür Ü, Alivov Ya I, Liu C, Teke A, Reshchikov M A, Dogan S, Avrutin V, Cho S J & Morkoc H, *J Appl Phys*, 98 (2005) 041301.
4 Look D C, *Mater Sci Eng B*, 80 (2001) 383.
5 Rana N, Chand S & Gathania A K, *Int Nano Lett*, 6 (2016) 91.
6 Rana N, Chand S & Gathania A K, *J Mater Sci Mater Electron*, 27 (2016) 2504.
7 Rana N, Chand S & Gathania A K, *Ceram Int*, 41 (2015) 12032.
8 Rana N, Chand S & Gathania A K, *Phys Scr*, 90 (2015) 85502.
9 Prado A G S, Bolzon L B, Pedroso C P, Moura A O & Costa L L, *Appl Catal B Environ*, 82 (2008) 219.
10 Dhiman N, Singh B P & Gathania A K, *J Nanophotonics*, 6 (2012) 063511.
11 Sharma A, Rao P, Mathur R P & Ameta S C, *J Photochem Photobiol :A Chem*, 86 (1995) 197.
12 Kormann C, Bahnemann D W & Hoffmann M R, *Environ Sci Technol*, 22 (1988) 798.
13 Khodja A A, Sehili T, Pilichowski J F & Boule P, *J Photochem Photobiol :A Chem*, 141 (2001) 231.
14 Poulios I & Tsachpinis I, *J Chem Technol Biotechnol*, 74 (1999) 349.
15 Sakthivel S, Neppolian B, Shankar M V, Arabindoo B, Palanichamy M & Murugesan V, *Sol Energy Mater Sol Cells*, 77 (2003) 65.
16 Hoffman A J, Carraway E R & Hoffmann M R, *Environ Sci Technol*, 28 (1994) 776.
17 Lin C C, Lin W H & Li Y Y, *J Phys D Appl Phys*, 41 (2008) 225411.
18 Zhang J, Sun L D, Jiang X C, Liao C S & Yan C H, *Cryst Growth Design*, 4 (2004) 309.
19 Maensiri S, Laokul P & Promarak V, *J Cryst Growth*, 289 (2006) 102.
20 Wu Y, Xi Z, Zhang G, Zhang J & Guo D, *Cryst Growth Des*, 8 (2008) 2646.
21 Height M J, Mädler L, Pratsinis S E & Krumeich F, *Chem Mater*, 18 (2006) 572.
22 Li W J, Shi E W, Zhong W Z & Yin Z W, *J Cryst Growth*, 203 (1999) 186.
23 Hu Y & Chen H J, *J Nanoparticle Res*, 10 (2008) 401.
24 Guzman S S, Jayan B R, Rosa E, Castro A T, Gonzalez V G & Yacaman M J, *Mater Chem Phys*, 115 (2009) 172.
25 Biswick T, Jones W, Pacuła A, Serwicka E & Podobinski J, *Solid State Sci*, 11 (2009) 330.
26 Cuscó R, Alarcón-Lladó E, Ibáñez J, Artús L, Jiménez J, Wang B & Callahan M J, *Phys Rev B,* 75 (2007) 165202.
27 Kwon Y J, Kim K H, Lim C S & Shim K B, *J Ceramic Proc Res*, 3 (2002) 146.
28 Xiong G, Pal U, Serrano J G, Ucer K B & Williams R T, *Phys Status Solidi*, 3 (2006) 3577.
29 Tauc J & Menth A, *J Non Cryst Solids*, 8 (1972) 569.
30 Hong R, Huang J, He H, Fan Z & Shao J, *Appl Surf Sci*, 242 (2005) 346.
31 Talebian N & Nilforoushan M R, *Thin Solid Films*, 518 (2010) 2210.
32 Du P F, Song L X, Xiong J, Xi Z Q, Chen J J, Gao L H & Wang N Y, *J Nanosci Nanotechnol*, 11 (2011) 7723.

33 Gaya U I & Abdullah A H, *J Photochem Photobiol C :Photochem Rev,* 9 (2008) 1.
34 Sokker H H, El-Sawy N M, Hassan M A & El-Anadouli B E, *J Hazard Mater*, 190 (2011) 359.
35 Yuvakkumar R, Suresh J, Nathanael A J, Sundrarajan M & Hong S I, *Mater Sci Eng C*, 41 (2014) 17.
36 Bhuyan T, Mishra K, Khanuja M, Prasad R & Varma A, *Mater Sci Semicond Process*, 32 (2015) 55.
37 Fu G, Vary P S & Lin C T, *J Phys Chem B*, 109 (2005) 8889.
38 Sirelkhatim A, Mahmud S, Seeni A, Kaus N H M, Ann L C, Bakhori S K M, Hasan H & Mohamad D*, Nano-Micro Lett*, 7 (2015) 219.